Proceedings World Geothermal Congress 2020+1
Reykjavik, Iceland, April - October 2021

Application of ASTER Satellite Imagery to Delineate Hydrothermal Alteration Zones Associated with Geothermal Resource: A Case Study of Olkaria and Eburru Geothermal System, Kenya Rift

Mathew Kamau, Fred Wekesa

mwkamau@kengen.co.ke

fwekesa@kengen.co.ke

Keywords: *Geothermal, ASTER, Hydrothermal minerals, Remote sensing, Olkaria, Eburru*

ABSTRACT

Olkaria and Eburru geothermal prospects are within the central region of the Kenyan rift. Exploration for geothermal resources in these prospects has conventionally been done using geophysical, geochemical and geological exploration techniques. However, advance in remote sensing technology and digital image processing techniques, has provided significant tools for mapping surface distribution of important hydrothermal minerals and alteration zones associated with geothermal resource. Subsequently, information derived from remote sensing data can be used in early stages of geothermal exploration thus reducing time and cost required for exploration. The Advanced Spaceborne Thermal Emission and Reflection Radiometer (ASTER) optical and thermal satellite sensor is one of the remote sensing instruments that has been used to optimize geothermal exploration techniques by providing free data for mapping hydrothermal alteration minerals and alteration zones associated with geothermal resource. It has a total of 14 bands measuring reflected radiation in Visible Near Infrared (VNIR) with 3 bands, Short Wave Infrared (SWIR) 6 bands and Thermal Infrared (TIR). This study uses VNIR-SWIR ASTER data to map hydrothermal alteration minerals and dominant alteration zones in the study areas. Image processing techniques used for this study includes; color composite, logical algorithms, band ratios and Relative Band Depth (RBD). Results shows successful mapping of alteration zones with argillic-phyllic alteration dominating in the area of study.

1. INTRODUCTION

Use of multispectral image data have successfully been used for mapping hydrothermal alteration minerals particularly since the launch of the Landsat Thematic Mapper instrument(Tommaso & Rubinstein, 2007). This was possible because Landsat came with two addition bands in the SWIR region in which many clay minerals have significant diagnostic absorption features. A big success in geological remote sensing was in the year 1999 when ASTER a multispectral imager was launched by Japan's Ministry of Economy, Trade and Industry (METI) and National Aeronautics and Space Administration (NASA). It consist of three separate subsystems with a total of 14 bands in VNIR, SWIR and TIR wavelength range of the electromagnetic system (Testa et al, 2018).

VNIR (B1-B3) which ranges from 0.52-0.86µm are useful for detecting iron oxides and vegetation cover, SWIR(B4-B9) ranging from 1.60-2.430µm useful for mapping clays minerals with Al-OH, Mg-OH, Fe-OH and carbonate absorption features while TIR (B10-B14) ranging between 8.125-11.65µm are useful for defining surface temperature and characterizing silicate rocks (Hewson et al., 2019). The instrument has swath width of 60 km (60kmx60km scene) with a recurrent time of 16 days. VNIR bands and SWIR bands has spatial resolution of 15m and 30m respectively while TIR bands have spatial resolution of 90m (Figure 1). Increase in number of spectral bands compared to Landsat TM make it more accurate for geological mapping.

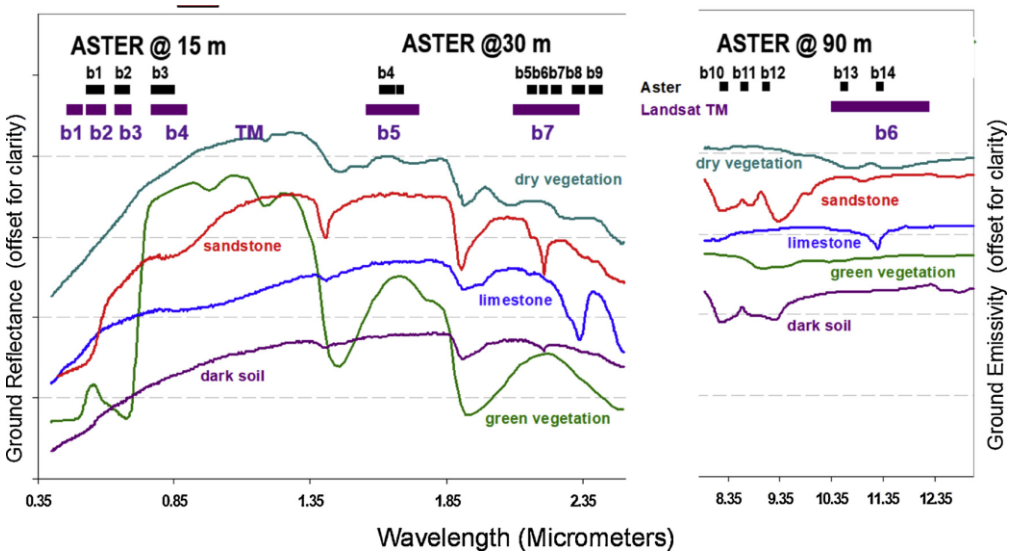

Figure 1: Reflectance spectrum of common surface materials and comparison of occurrence of ASTER and Landsat TM bands together with spatial resolution (Hewson et al., 2019).

Previously, various studies have used ASTER data to identify and delineate hydrothermal alteration mineral and alteration zones for mineral and geothermal resource exploration. For instance Pour & Hashim, (2011) highlighted use of ASTER SWIR data as a tool for identification of hydrothermal alteration minerals such as alunite, kaolinite ,calcite ,dolomite, chlorite talc and muscovite. Rahimi et al, (2018), used ASTER data to identify potential alteration zones on Microwave ridge in Western-Central British Columbia. Hewson et al., (2019, used ASTER day and nighttime data to map geothermal and mineral mapping in the East Africa.

To achieve this, several spectral processing techniques on ASTER images have been used previously. For example, Tommaso & Rubinstein,(2007) used band combination and band ratio transformation to map hydrothermal alteration minerals in Infiernillo porphyry deposit, Argentina. Ghosh et al, (2016), used band ratio and relative band depth to delineate alteration related clay minerals in Sakoli belt, Maharashtra. Hecker et al, (2017) used aster band parameters such as band ratioing and band math for geothermal targeting in Flores island in Indonesia.

During early stages of geothermal exploration, high turnaround time and cost is involved especially for highly in accessible areas. In this case, satellite images can be used to fill the gap by providing information for larger area in inaccessible regions and help delineate potential areas from non-interesting areas for further detailed investigation. In this regard, this study uses ASTER data to delineate potential geothermal resource areas in Olkaria and Eburru prospect. VNIR&SWIR spectral data were processed to extract most relevant and useful information. Color composite images (RGB), Normalized Different Vegetation Index (NDVI), logical operator algorithms, band ratio and Relative Band Depth were used in this study.

2. AREA OF STUDY

The study areas (Figure 2) are located on the central region of the Kenyan Rift valley. Olkaria geothermal area is located to the south of L. Naivasha about 100km NW of Nairobi (Omenda, 1998), while Eburru prospect is located about 40 km NW of Olkaria prospect(Omenda & Karingithi, 1993). Currently, Olkaria geothermal prospect has a geothermal installed electricity capacity of 705MW while Eburru is producing of 2.4 MW.

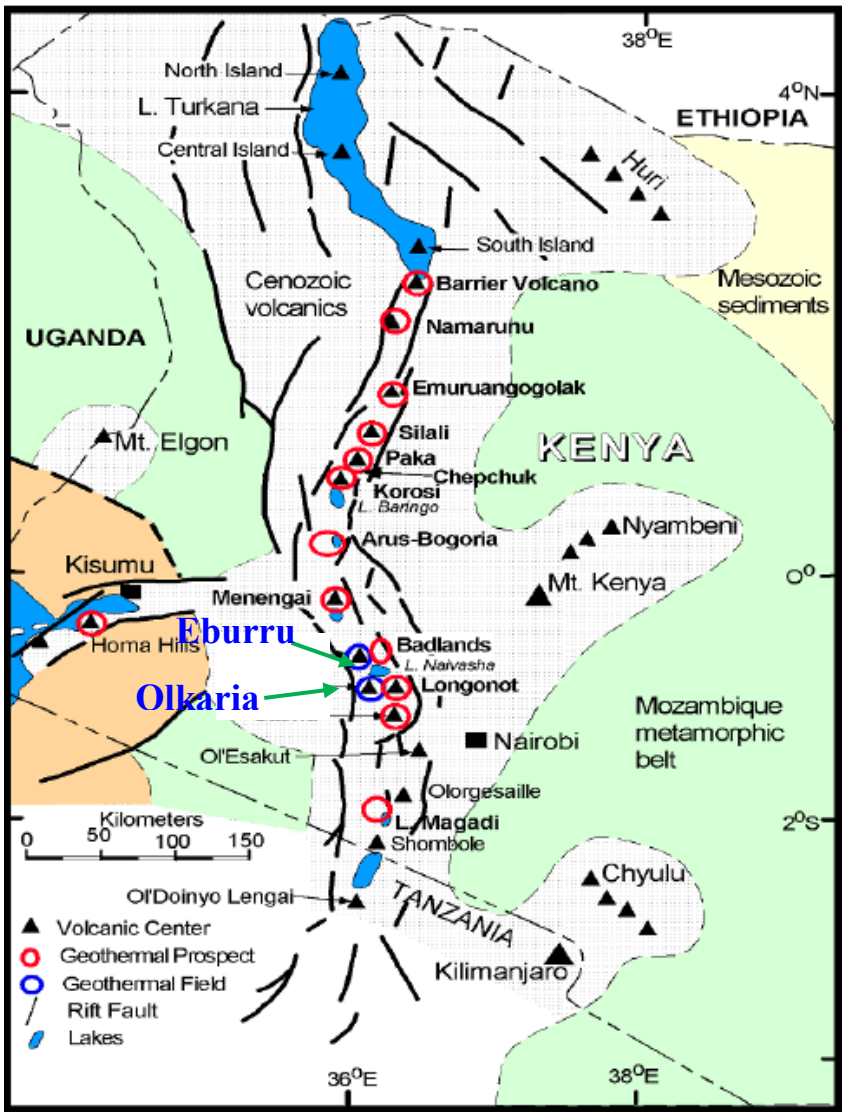

Figure 2: Location of Olkaria and Eburru geothermal prospect on the floor of the Kenyan rift (Simiyu, 2010)

3. GEOLOGICAL SETTING

3.1 Olkaria prospect

Olkaria geothermal prospect is characterized by numerous Quaternary volcanic centers, including a ring of volcanic domes on the east and the south sides of the field area (Omenda, 1998). The surface geology is dominated by rhyolitic lavas and pyroclastic rocks (Figure 3) whereas beneath it, a series of basalts, trachyte and pyroclastic units above the Proterozoic basement rock. Structurally, volcanic units are cut by numerous faults which can be mapped on the evidence of aligned features such as hot ground, extrusion centers and craters Notable among this fault are Ololbutot and Olkaria Faults (Munyiri, 2016)

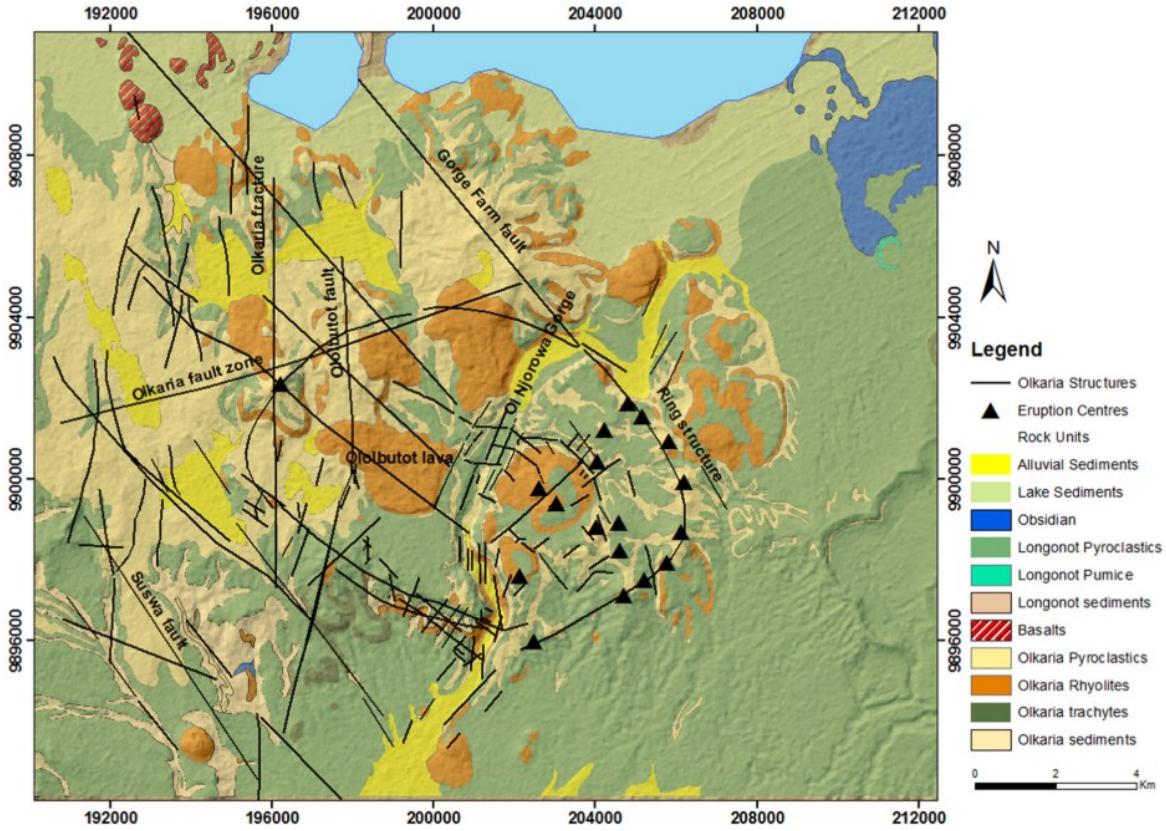

Figure 3: Surface geology and structural features within Olkaria geothermal prospect (Munyiri, 2016)

3.2 Eburru prospect

The Eburru volcanic complex is an almost east-west trending ridge with an area of approximately 470 km^2 (Velador et al, 2003). It is made of two topographic highs in the west and the east. Each of these topographic entities is a ring structure. It is part of volcanic belt of peralkaline rocks trending in the NS direction and extending to the south of Suswa volcanic complex. It is characterized by highly evolved trachytic and rhyolitic compositions which differ in detail from those erupted at Longonot and Olkaria in that they are richer in total iron and lower in alumina(Clarke, Woodhall, 1990). The surface rocks comprise mainly Quaternary pantelleritic lava flows and volcanic ash (Muchemi, 1998). Trachytic lava flows occur on the slopes of the eastern volcano and on the plains. Above 1400 m asl are rhyolites and pyroclastics while below this, the dominant rocks are trachyte and minor basaltic, rhyolite and pyroclastic flows (Figure 4)

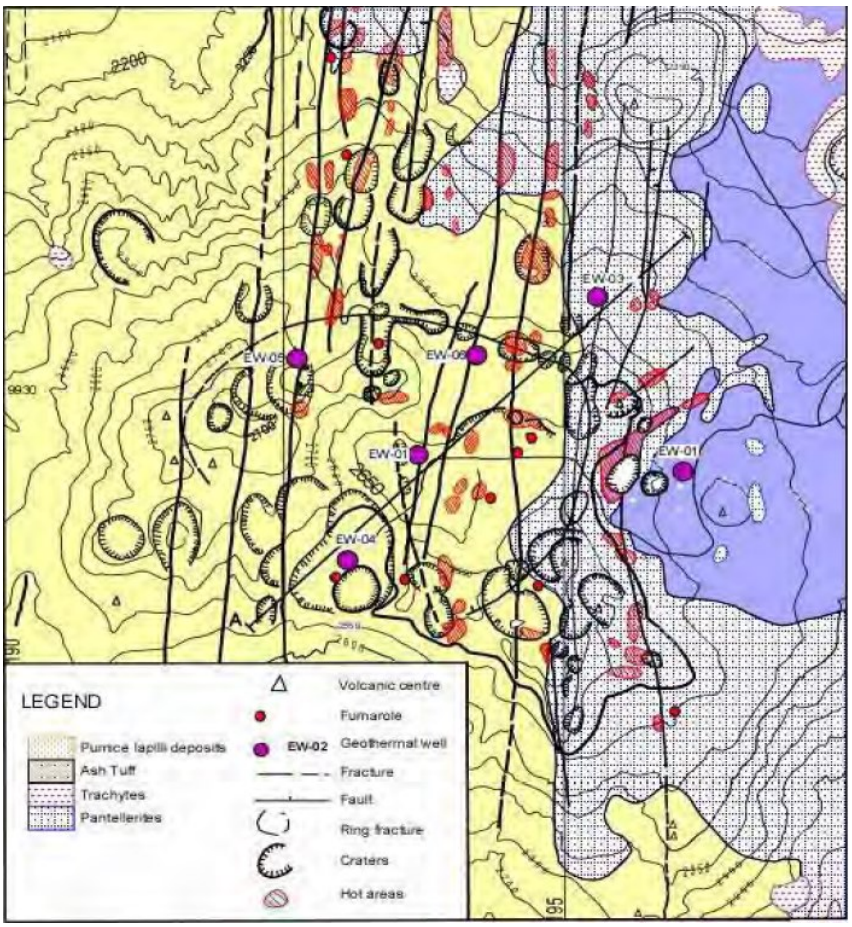

Figure 4: Surface geology map of Eburru geothermal prospect (Clarke, Woodhall, 1990)

4. DATA SET AND METHODOLOGY

4.1 ASTER Data

Two scenes of daytime ASTER Surface Reflectance VNIR and Crosstalk corrected SWIR (AST_07XT) acquired on 15th October 2004 was used for this study. These data contain measures of the fraction of the incoming solar radiation reflected from the earth surface to the ASTER instrument. It was retrieved from https://search.earthdata.nasa.gov/search and was acquired having been corrected for both atmospheric and viewing geometry effects. Equally, crosstalk corrected surface reflectance was chosen in order to minimize interference of the reflected light between SWIR arrays detectors. The scenes were chosen on a cloud-free day and was already georeferenced to the UTM zone 37 S projection using the WGS-84 datum.

4.2 Methodology

The data was first pre-processed by layer stacking of VNIR& SWIR resulting into a 9 band image data and then resizing (spatial subset) to the area of interest. This was important because it allows multiple combination of bands from different wavelength range thus allowing in-depth qualitative analysis and quick detection of alteration minerals.

4.1.1 Color composite

Color composite images were used to acquire general information about the land cover and lithology in the study area. Red, Green, Blue (RGB): 3-2-1, 6-3-1 and 4-6-8 were used for this study. They were used as a rough guide to detect main lithological and alteration differences together with delineating highly vegetated areas.

4.1.2 Normalized Difference Vegetation Index (NDVI) calculation

NDVI is a simple numerical indicator that can be used to measure vegetation cover change. It is calculated by the equation;

$$NDVI = \frac{NIR - RED}{NIR + RED}$$

Where NIR and RED stand for the reflectance values in the near infrared and visible red spectral regions respectively (Bolanio et al, 2015). The result is a ratio with possible values between -1 and +1. Values above 0 are generally considered vegetated with higher values indicating denser vegetations. For this study, NDVI map was created using band 2&3 using EVNI/Transform/NDVI. Threshold used for non-vegetated areas was between 0-0.4 while those with value <0 were pixel under water and had no data.

4.1.3 Logical Operator Algorithms

This was aimed at to map hydrothermally altered Al-OH spectral absorption features associated with alunite, kaolinite and sericite-muscovite. As suggested by Mars, (2013), this was filtered using logical operators ((float(b3)/b2) le 1.35) and (b4 gt 260) and ((float(b4)/b5) gt 1.25)and ((float(b5)/b6) le 1.05) and ((float(b7)/b6) ge 1.03).

4.1.4 Band Ratio

It is a technique where the procedure involves the division of two bands, where the bands with high reflectance features of the given material is assigned numerator while the absorption features for the same material is assigned the denominator (Rouskov et al, 2014). The technique improves the contrast and enhances compositional information by highlighting spectral differences between bands and the reduction of the topographic effects. For this study, band ratio 4/6 was used as an indicator for hydrothermal alteration. Clay mineral show high reflectance in band 4 and low reflectance in band 6.

4.1.5 Relative Absorption Band Depth (RBD)

In this case, a band depth image is created by dividing the sum of the two highest reflectance spectral bands which may be in a sequence in reflectance channel or not by the lowest absorption features (Figure 5).The resultant product is a one band image with pixel values which are proportional to the depth of the absorption feature at the wavelength of the reflectance minimum. The Relative Band Depth (RBD) detects the clay bearing groups of minerals based on the location and depth of the absorption's features. In this study, band depth *(b4+b6)/b5* was used to highlight kaolinite/alunite, *(b5+b7)/b6* was used to highlight sericite/illite/muscovite and (b7+b9)/b8 to map calcite/epidote/calcite.

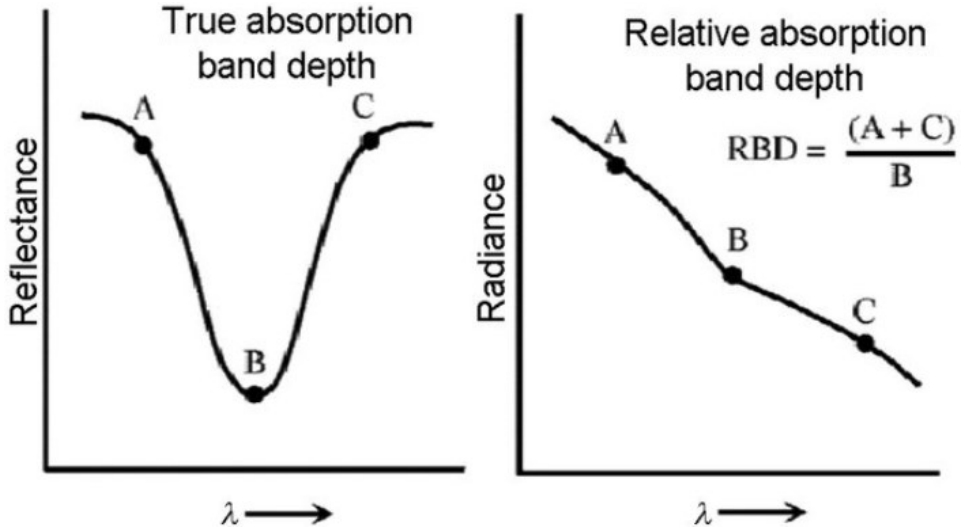

Figure 5: True and relative absorption band depths (Banerjee et al, 2019)

5. RESULTS AND DISCUSSION

5.1 Color composite images: ASTER band combinations in RGB (red, green, blue)

RGB composite image for band 3-2-1 has been prepared for the study area (Figure 6 a). The red color clearly mapped areas which are highly vegetated. On the other hand, color composite image for band 4-6-8 composite images (Figure 6b) was typically sued to show argillic and phyllic alteration. The result shows slight discrimination with the argillic and phyllic altered rocks in amethystine tones.

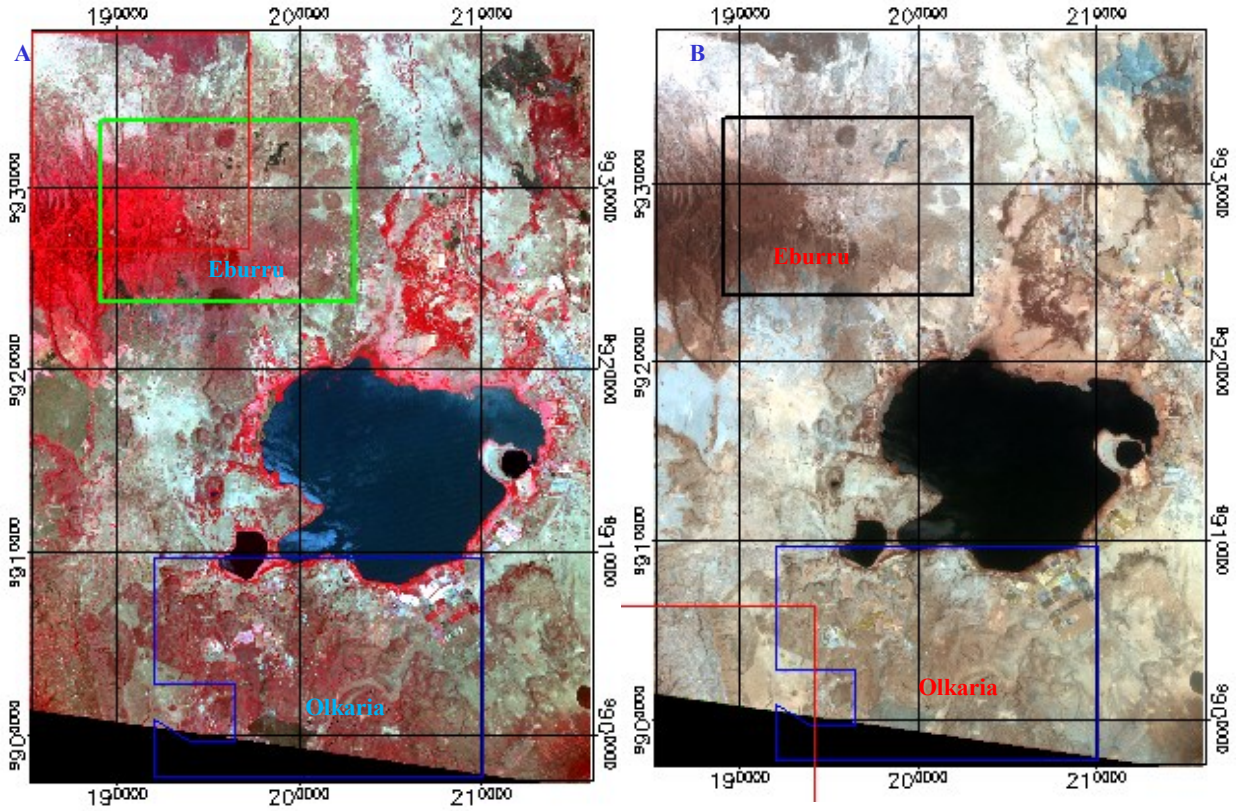

Figure 6: Color composite images for (A) band 3-2-1 and (B) band 4-6-8

5.2 Normalized Difference Vegetation Index (NDVI) map

The map was prepared using band 2&3 using ENVI/ Transform/NDVI algorithm (Figure 7a). The vegetated areas are represented by red areas. 0-0.4 thresholds were used to map vegetated areas while <0 pixels under water had no data.

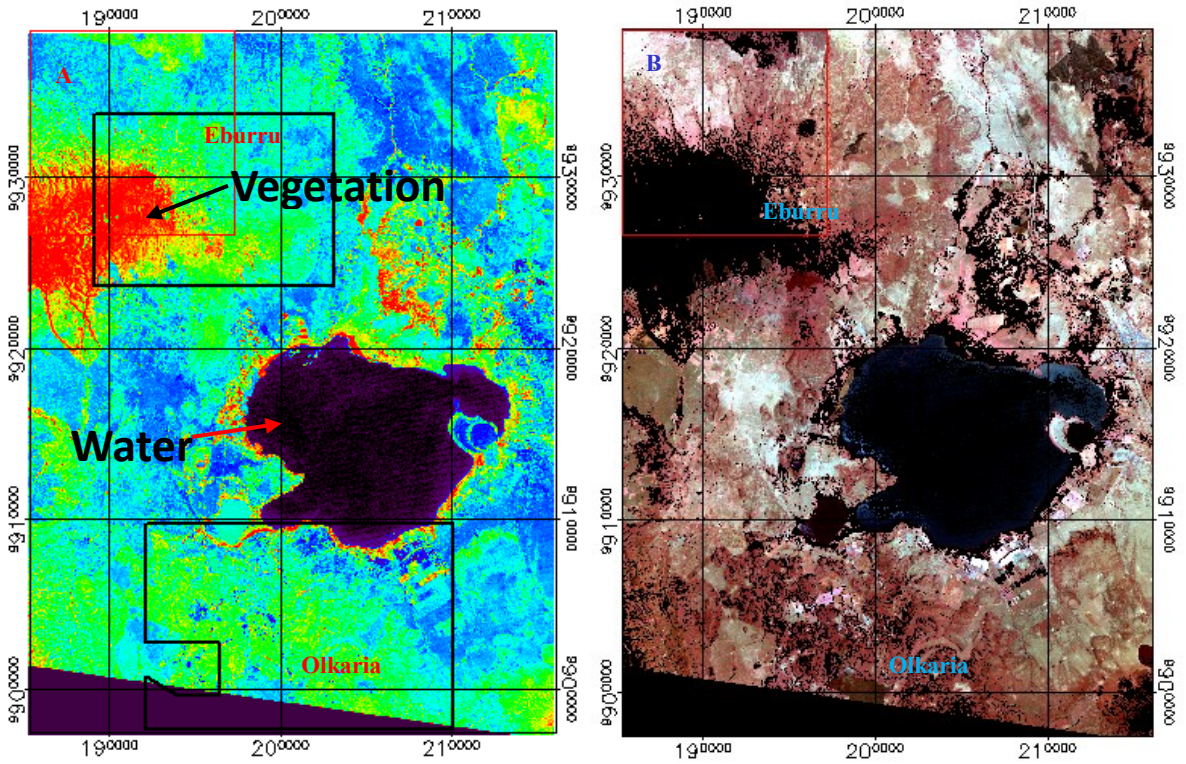

Figure 7: NDVI map(A) and (B) map showing masked vegetation and water pixels

5.3 Logical Operator Algorithms

This technique managed to map pixels of phyllic and argillic hydrothermal alteration mineral whose deepest absorption features occurs approximately at 2.16µm. From the result, very few pixels were mapped as argillic altered areas (Figure 8).

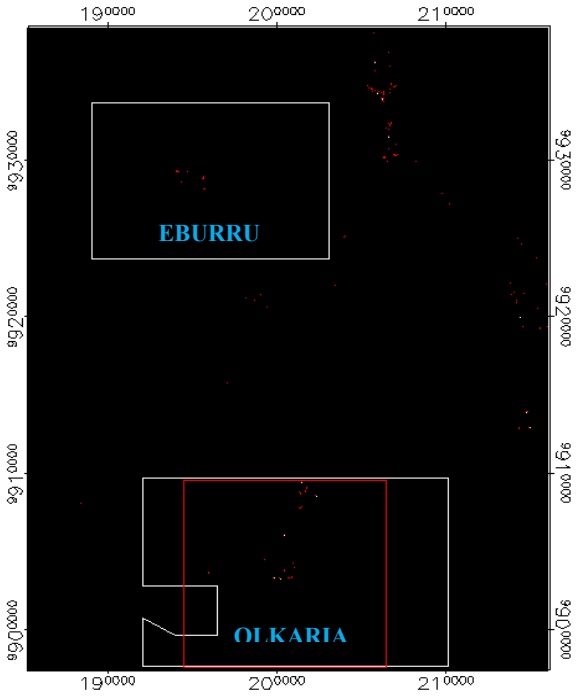

Figure 8: Red pixels shows area with argillic/ phyllic alteration

5.4 Band ratio

From the results, SWIR band ratio 4/6 was found to be a good indicator for hydrothermal alteration minerals. Characteristically, clay minerals show high reflectance in band 4 and low reflectance in band 6. A threshold of between 1.5-2.3 was used to extract yellow colored pixels which are indicator of alteration zones. The result is consistent with RGB 4-6-8 color composite image.

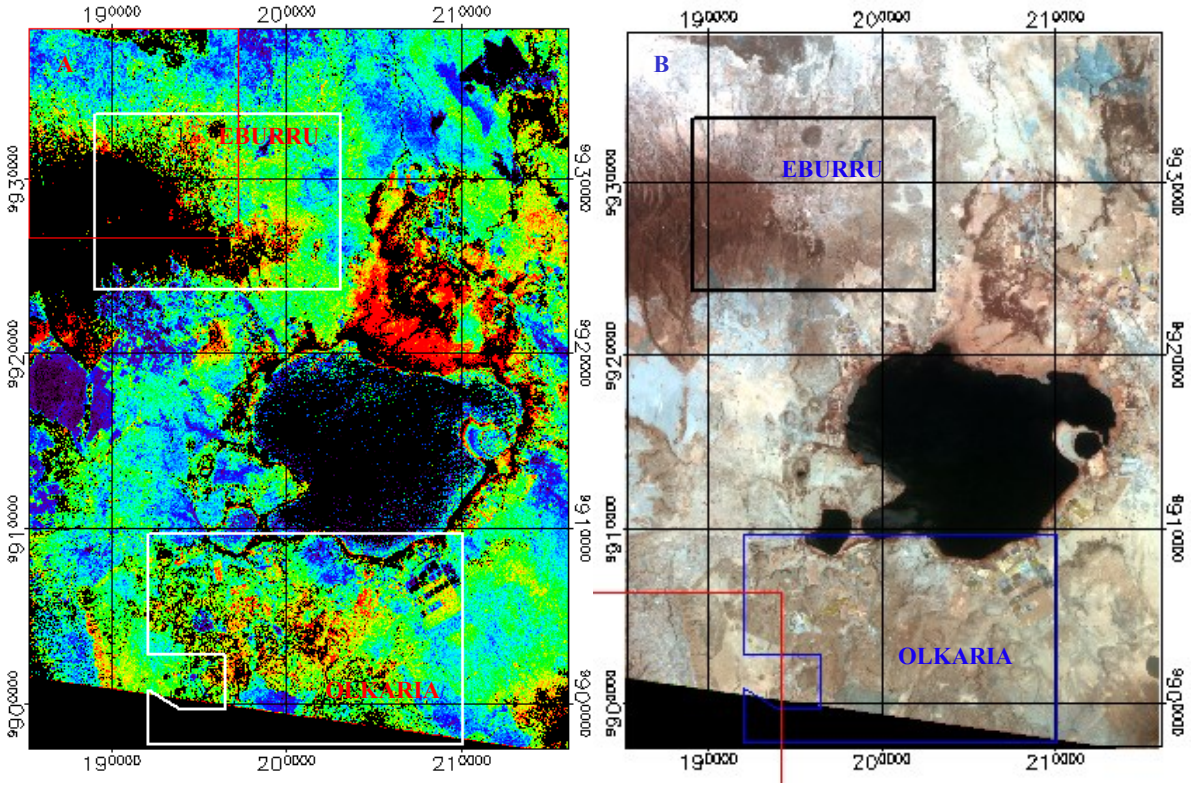

Figure 9: B4/B6 alteration image (A) compared with color composite image for band 4-6-8

5.5 Relative Band Depth (RBD)

The RBD detects clay bearing group of minerals based on the location and depth of the absorption features. RBD images sensitive to kaolinite/ alunite, sericite/illite/ muscovite and calcite/epidote /chlorite was used to identify them in the study area. Results shows the most dominant alteration minerals are either alunite/ kaolinite (Figure 10a). Very few pixels were mapped indicating presence of illite/muscovite in the study area (Figure 10b). However, zones of alteration associated with either calcite/epidote/ chlorite were identified in Olkaria central region (Figure 10c). In addition, a Relative band Depth of argillic, phyllic and propylitic alterations in RGB image was generated. In this case: Red= kaolinite/alunite group (b4+b6)/b5, Green = illite group (b5+b7)/b6, Blue = chlorite group (b7+b9)/b8 (Figure 10d). Magenta color shows high values in red and blue band which indicate a mixture of kaolinite and chlorite group of minerals. Green area shows phyllic alteration associated with illite, sericite and muscovite and lastly, cyan color indicates high values in green and blue bands. However, this is interpreted as an anomaly since the pixels falls on water area of L. Naivasha.

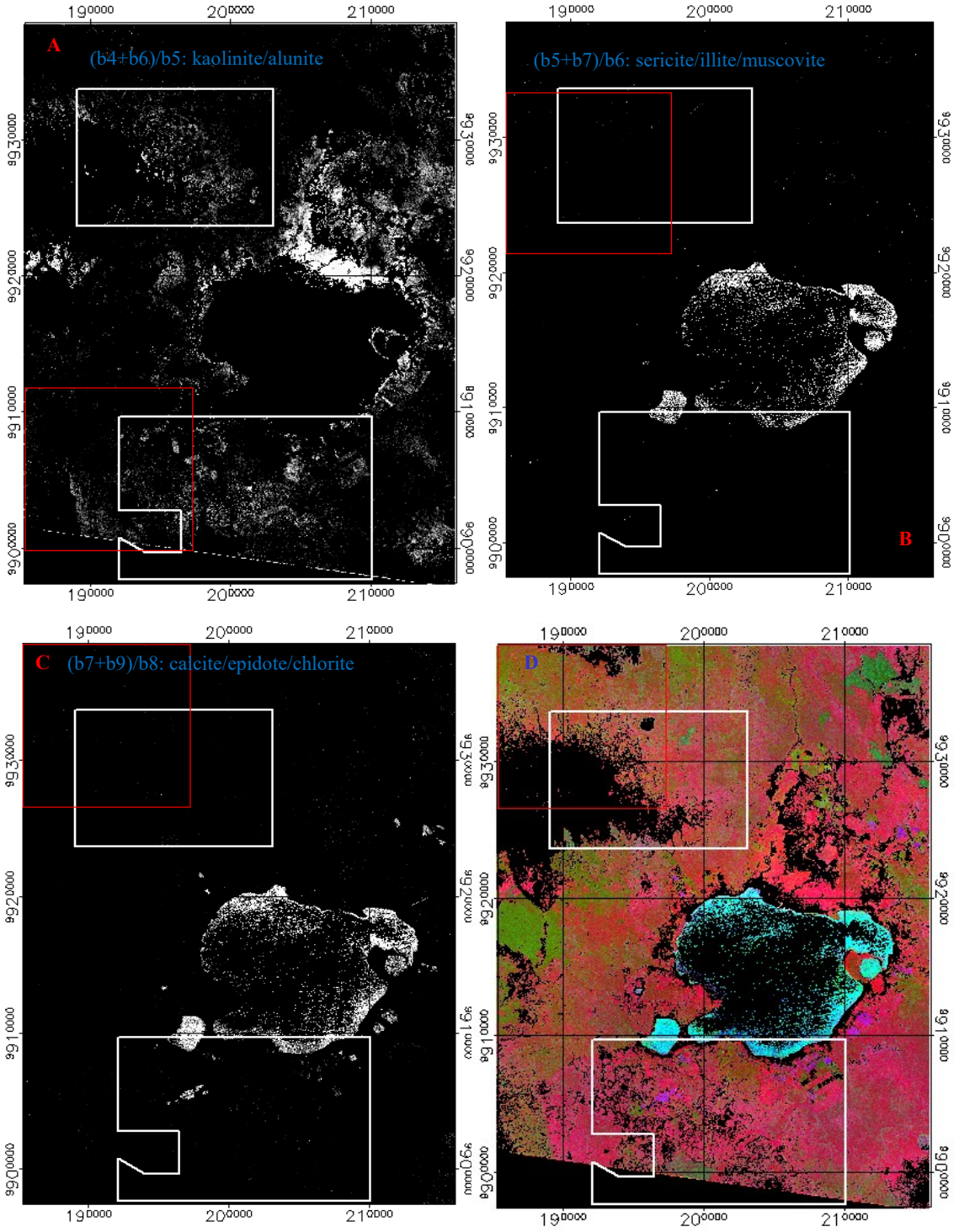

Figure 10: RBD for mapping kaolinite/alunite (B) for mapping sericite/illite/muscovite(C) for mapping calcite/ epidote/chlorite(D) RGB images from the three RBD depths

6. CONCLUSION

VNIR and SWIR ASTER data effectively identified and delineated alteration minerals assemblages in the area of study. Image processing tools such as colour composite, logical algorithms, band ratio and RBD on ASTER data has effectively delineated hydrothermal alteration minerals assemblages and alteration zones in the study area. The results of this study indicate presence of group of minerals such as kaolinite/alunite, sericite/illite/muscovite and calcite/epidote/chlorite. The alteration zonation mapped with the use of ASTER data includes argillic, phyllic and propylitic. Results derived from this study confirm ASTER images can be used as tool for initial steps of geothermal exploration. High accuracy maps derived from the processed images can allow delineation of alteration zones of pontential geothermal resource thus reducing time and cost required for field exploraion and evaluation procedure.

7. RECOMMENDATION

Fieldwork is highly recommended to validate the results derived from the study. Future study to include TIR bands to assess surface temperature anomalies in the study area.

ACKNOWLEDGMENTS

I appreciate the Land Processes Distributed Active Archive Centre (LPDAAC) for providing free access to data used for this study. Special thanks to Amarjargal Davaardorj for help offered during processing of the data used for this study.

REFERENCES

Banerjee, K., Jain, M. K., Jeyaseelan, A. T., & Panda, S. (2019). Landsat 8 OLI data for identification of hydrothermal alteration zone in Singhbhum Shear Zone using successive band depth difference technique - A new image processing approach. *Current Science*, *116*(10), 1639–1647. https://doi.org/10.18520/cs/v116/i10/1639-1647

Bolanio, K. P., Santillan, M. M., Santillan, J. R., & Daguil, R. C. (2015). Using normalized difference vegetation index (NDVI) to assess vegetation cover change in mining areas of tubay Agusan del norte. *ACRS 2015 - 36th Asian Conference on Remote Sensing: Fostering Resilient Growth in Asia, Proceedings*, (October).

Clarke, Woodhall, A. & D. (1990). *Geological, volcanological and hydrogeological controls on the occurrence of geothermal activity sorrounding Lake Naivasha, Kenya*. Nairobi.

Ghosh, U. K., Kesari, M. P., & Naik, K. K. (2016). Digital image processing of multispectral ASTER imagery for delineation of alteration and related clay minerals in Sausar Belt-a case study. *Indian Journal of Geosciences*, *70*(1), 49–58.

Hecker, C., Hewson, R., Setianto, A., Saepuloh, A., & van der Meer, F. D. (2017). Multi-source remote sensing data analysis for geothermal targeting on Flores island. *Proceedings The 5th Indonesia International Geothermal Convention & Exhibition (IIGCE) 2017*, (August), 1–7.

Hewson, R., Mshiu, E., Hecker, C., van der Werff, H., van Ruitenbeek, F., Alkema, D., & van der Meer, F. (2019). The application of day and night time ASTER satellite imagery for geothermal and mineral mapping in East Africa. *International Journal of Applied Earth Observation and Geoinformation*, (October), 101991. https://doi.org/10.1016/j.jag.2019.101991

Mars, J. (2013). Hydrothemal Alteration Maps of the Central and Southern Basin and Range Province of the United States Compiled from Advnaced Spaceborne Thermal Emission and Reflection Radiometer(ASTER) Data.pdf. Retrieved from https://pubs.usgs.gov/of/2013/1139/of2013-1139.pdf

Muchemi, G. (1998). Geothermal Exploration in the Kenyan Rift.pdf. Retrieved from https://orkustofnun.is/gogn/unu-gtp-20-ann/UNU-GTP-20-14.pdf

Munyiri, S. K. (2016). *Structural Mapping of Olkaria Domes Geothermal Field Using Geochemical Soil Gas Surveys , Remote Sensing and GIS. The School of Engineering and Natural Sciences, Faculty of Earth Sciences University of Iceland* (Vol. 7). Retrieved from http://dx.doi.org/10.1016/j.proeps.2013.03.220%0Ahttp://theargeo.org/fullpapers/Olkaria Geothermal Field reservoir response after 35 years of production.pdf

Omenda, & Karingithi, C. (1993). Hydrothermal Model Of Eburru Geothermal Field, Kenya. *Geothermal Resource Council Transactions*, *17*(4), 155–160. https://doi.org/10.1080/09640560701402075

Omenda, P. A. (1998). The geology and structural controls of the Olkaria geothermal system, Kenya. *Geothermics*, *27*(1), 55–74. https://doi.org/10.1016/S0375-6505(97)00028-X

Pour, A. B., & Hashim, M. (2011). Application of advanced spaceborne thermal emission and reflection radiometer (ASTER) data in geological mapping, *6*(33), 7657–7668.

Rahimi, Angen, H. (2018). Application of ASTER Data to Identify Potential Alteration Zones on Microwave Ridge , Northeastern Search Project Area , West-Central British Columbia (part of NTS 093L).

Rouskov, K., Popov, K., & Stoykov, S. (2014). Some Applications of the Remote sensing in Geology by using ASTER Images. *Researchgate*, (January 2014).

Simiyu, S. M. (2010). Status of Geothermal Exploration in Kenya and Future Plans for Its Development. *World Geothermal Congress 2010*, (April), 25–29.

Testa, F. J., Villanueva, C., Cooke, D. R., & Zhang, L. (2018). Lithological and hydrothermal alteration mapping of epithermal, porphyry and tourmaline breccia districts in the argentine andes using ASTER imagery. *Remote Sensing*, *10*(2), 1–45. https://doi.org/10.3390/rs10020203

Tommaso, & Rubinstein, N. (2007). Hydrothermal alteration mapping using ASTER data in the Infiernillo porphyry deposit,

Argentina. *Ore Geology Reviews*, *32*(1–2), 275–290. https://doi.org/10.1016/j.oregeorev.2006.05.004

Velador, J, Omenda, P, Andrew, C. (2003). An Integrated Mapping and Remote Sensing Investigation of the Structural Control for Fumarole Location in the Eburru Volcanic Complex , Kenya Rift, (January). Retrieved from https://www.researchgate.net/publication/253796592_Geology_and_the_origin_of_trachytes_and_pantellerites_from_the_Eburru_volcanic_field_Kenya_Rift